LA-UR- **99-5820**

Title: | RASTER MAGNET SYSTEM FOR EXPANDING THE APT PROTON BEAM

Author(s): | Richard Sheffield, APT/TPO
Martin E. Schulze, APT/TPO-GA

Submitted to: | BREI/GA for Publication and for Internal/External Distribution

Los Alamos
NATIONAL LABORATORY

Form 836 (10/96)

APT
Accelerator
Production
of Tritium

Los Alamos
NATIONAL LABORATORY
Los Alamos, New Mexico 87545

Accelerator Production of Tritium Project Technical Note

Accelerator ED&D Program

Final Report: Raster Magnet System for Expanding the APT Proton Beam

September 1999

Title:

Raster Magnet System for Expanding the Apt Proton Beam

Document Number:

TPO-A14-G-TRT-X-00075
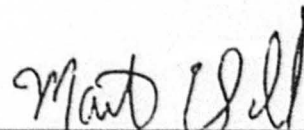
Category: 1

Abstract:

A method of expanding the 1700-MeV, 100-mA proton beam of the APT linear accelerator onto the 19-cm by 190-cm target has been devised using eight ferrite dipole magnets. These magnets deflect the beam in the x- and y-planes, and thereby paint the target area uniformly with a rastered pattern. Insulated Gate Bipolar Transistor-based power modulators drive the raster magnets with triangular current waveforms that are synchronized using voltage-controlled crystal oscillators and phase-locked loops. Redundant fault-detection circuits monitor both the ac magnet currents and magnetic fields to ensure proper operation. This paper presents the test results taken on an integrated prototype system, including eight magnets, the associated modulators, the master clock, and the fault detection circuitry.

Requester:

Team Lead

APT/TPO/GA

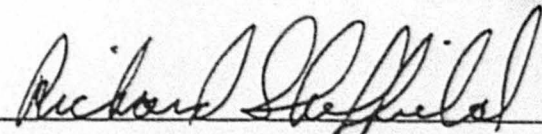Los Alamos National Laboratory

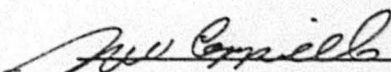Martin E. Schulze

Approvals:

Project Leader

APT/TPO

Richard Sheffield

Derivative Classifier

APT/TPO

Michael Cappiello

Contributors:

Project Guidance: Richard Sheffield (Los Alamos National Laboratory)

Report Preparation: M.E. Schulze, D.J. LeBon, R.E. Shafer (General Atomics, Los Alamos, NM), S. Chapelle, T. L. Smith (General Atomics, San Diego, CA)

Distribution List

Anderson, Jim	H816
Barber, Ron	H821
Baxter, Alan	C341
Cappiello, Mike	H816
Chan, Dominic	H816
Edwards, Jack	H816
Gambhir, Arun	C341
Johnson, Bob	H813
Kapernick, Rick	K551
Lisowski, Paul	H813
Maloy, Stuart	H809
McConnell, Steve	H816
McGill, John	H816
Parme, Laurence	C341
Quintana, Lawrence	H809
Schroder, Ron	C341
Tooker, Joe	H816
Van Tuyle, Greg	H813
Waters, Laurie	H816

**Accelerator
Production
of Tritium**

Final Report: Raster Magnet System for Expanding the APT Proton Beam

1   Introduction

The Accelerator for Production of Tritium (APT) project uses high-energy protons to produce spallation neutrons in a tritium-production target. The neutrons are captured by helium-3 nuclei and converted to tritium. The linear accelerator (linac) produces a 100-mA, 1700-MeV continuous wave (cw) (170-MW) proton beam, with transverse dimensions of about 1-cm $\times$ 2-cm root-mean-square (rms). The required beam *footprint* at the tritium-production target is 19 cm wide $\times$ 190 cm high. The required beam current uniformity in this footprint is about $\pm10\%$ or better. The purpose of the beam expander system is to transform the 1-cm $\times$ 2-cm proton beam to the 19-cm $\times$ 190-cm rectangular footprint.

2 System Requirements

Specific requirements and desirable features for the APT beam expander are listed below. Table 1 summarizes the performance requirements and the expected performance of the raster magnet system.

Rectangular expanded beam profile. The desired raster pattern is 19 cm wide × 190 cm high, with a horizontal penumbra not exceeding 3 cm on the sides and 10 cm on the top and bottom. Beam outside this 25-cm × 210-cm area misses the tungsten rods in the core, and therefore, reduces the overall tritium production efficiency.

Insensitivity to changes in beam parameters. Possible variations of the input beam include steering and focusing errors due to failure of a dipole or quadrupole element in the linac or changes in beam energy due to loss of a klystron. The expanded beam should be insensitive to these variations.

Tunability during full-power operation. Small variations in the expanded beam footprint size, steering, and rastered beam-spot size must be measurable and correctable during normal operation under full-power beam. Switching the beam to a tune-up beamstop or to low-duty-cycle operation for beam tuning is not acceptable. This means that the beam diagnostics must operate in a 170-MW cw beam.

Low beam losses. For hands-on maintenance of the beam expander components, beam losses should be limited to about 1 part in 10^8 (2 watts) per meter, or less. This, in turn, means large apertures.

No single-point failure modes. There should not be any failure modes that would cause the expanded beam to suddenly collapse to a ribbon or to a point. Component failures must result in graceful degradation of performance that can be easily detected, so appropriate action can be taken before beam current density limits on the target are exceeded.

Uniformity of expanded beam. The power density of the expanded beam should be flat within ±10% over the entire 19-cm × 190-cm footprint and should not exceed 65 kW/cm^2.

Thermal transients and stresses in target. Excessive thermal stresses can be caused by either temporal thermal transients or spatial thermal gradients. The raster system should have a sufficiently fine mesh and sufficiently high rastering frequencies to prevent these stresses.

Redundant fault detection. To reliably detect faults and not have erroneous fault signals that would unnecessarily shut down normal operation, the fault-detection circuit must have multiple redundant sensors and remain operational and reliable, even with single internal failures.

High reliability. To minimize beam shutdowns due to raster system failures, the system MTBF (mean time between failure) and MTTR (mean time to repair) have to be within acceptable limits.

Table 1. Raster Magnet System Performance Requirements

Parameter	Requirement	Performance
Footprint shape	Rectangular, 19-cm × 190-cm	By design
Beam outside 25-cm × 210-cm frame	None	<0.002% (simulation)
Footprint sensitivity to emittance changes	Minimal	<0.05% per % change (horizontal), <0.001% per % change (vertical)
Footprint sensitivity to beam momentum changes	Minimal	About 1% per % change in momentum
Tunability	Footprint size and centering adjustable during full power operation	Yes
Footprint size	<±0.5 cm (h); 1 cm (v)	<±0.5 cm (h); 1 cm (v)
Footprint centering	<±0.5 cm (h); 1 cm (v)	<±0.5 cm (h); 1 cm (v)
Beam losses along beamline	<1 nA per meter	Yes (due only to nuclear scattering on residual gas)
Single-point failure modes	None	Single-point failures cause only graceful degradation of performance
Uniformity of expanded beam	Better than ±10%	Less than ±2% variation
Thermal transients in target	Minimal	<±3°C repetitive
Fault detection system	Redundant, no single-point failure modes	Yes, 4 parallel independent systems, with 3 out of 4 logic.
Availability	>99.9%	Yes. MTBF >3500 hours, MTTR <2 hours

APT
Accelerator
Production
of Tritium

3 Basis For Design

In 1990, a beam expander design based on the use of nonlinear magnetic fields was chosen for APT.[1-3] The nonlinear expander design remained as the APT baseline design until 1997, when beam simulations showed that the nonlinear magnet design exhibited excessive sensitivity to the input beam parameters, and the simulated beam losses in the small nonlinear magnet apertures were unacceptably high.

A prototype high-frequency raster magnet and power supply based on insulated gate bipolar transistors (IGBTs) was demonstrated in 1997[4] and became the basis for a proposal to replace the nonlinear magnet beam expander design. A prototype eight-magnet raster system was built and tested in 1998 and became the baseline design for the APT beam expander.

The proposed design included eight raster magnets (four in each plane) using two close-ratio, nonharmonic frequencies to produce two triangular current waveforms, resulting in a fine-mesh raster pattern. An example of 13×16 and 23×26 raster meshes are shown in Fig. 1. The mesh size is adjustable by changing the x-y frequency ratio, and is chosen so that the mesh is filled in by the dimensions of the rastered beam spot.
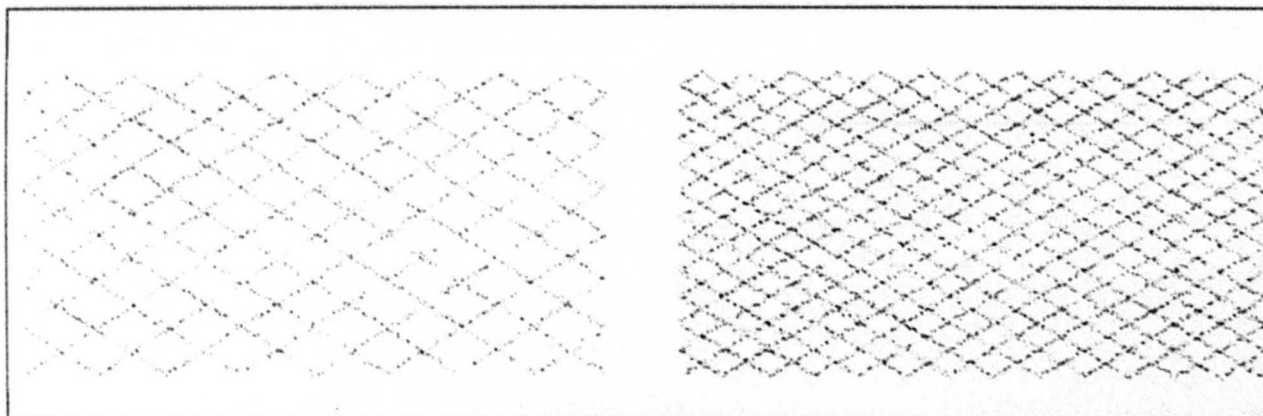

Figure 1. 13×16 and 23×26 mesh raster patterns

Accelerator
Production
of Tritium

4   Raster System Overview

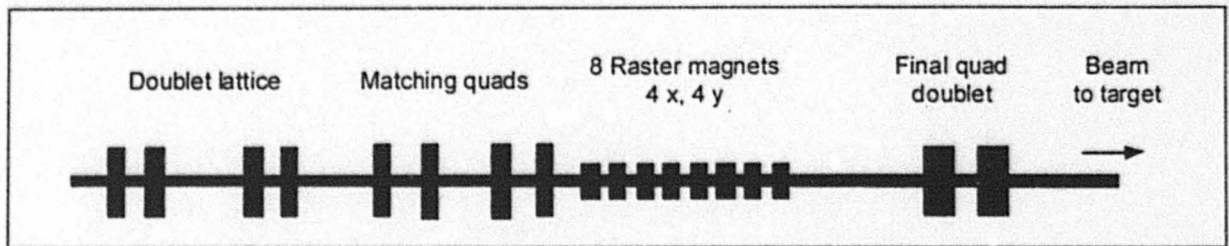The raster beam expander system is made up of three major magnet subsystems, as shown in Fig. 2.

Figure 2. The beam expansion system.

The four-quadrupole matching section matches the 1-mm × 2-mm input beam into the raster magnet section. The settings on these quadrupoles determine the rastered beam-spot size (about 1 cm × 2 cm rms) at the tritium-production target.

The eight-raster-magnet section deflects the beam in x and y to produce a rectangular raster pattern about 10 cm square in the quadrupole doublet lens.

The quadrupole doublet (objective) lens then focuses the beam-spot divergence and the deflections produced by the raster magnets onto the 19-cm-wide × 190-cm-high footprint at the tritium-production target.

The expansion chamber is a 25-m-long vacuum chamber in which the rastered beam expands to the 19-cm × 190-cm footprint when it reaches the tritium-production target. There is a double-waist (simultaneous vertical and horizontal waist) in the expanding beam about 5 m downstream of the quadrupole doublet, where a collimator will be placed to stop backstreaming neutrons. Loss of beam focus due to quadrupole failure will be intercepted by this collimator.

The arrangement of the eight raster magnets is shown in Fig. 3. The horizontal raster magnets are placed upstream of the vertical raster magnets to minimize the raster magnet apertures and to reduce the sensitivity to single-magnet failures.
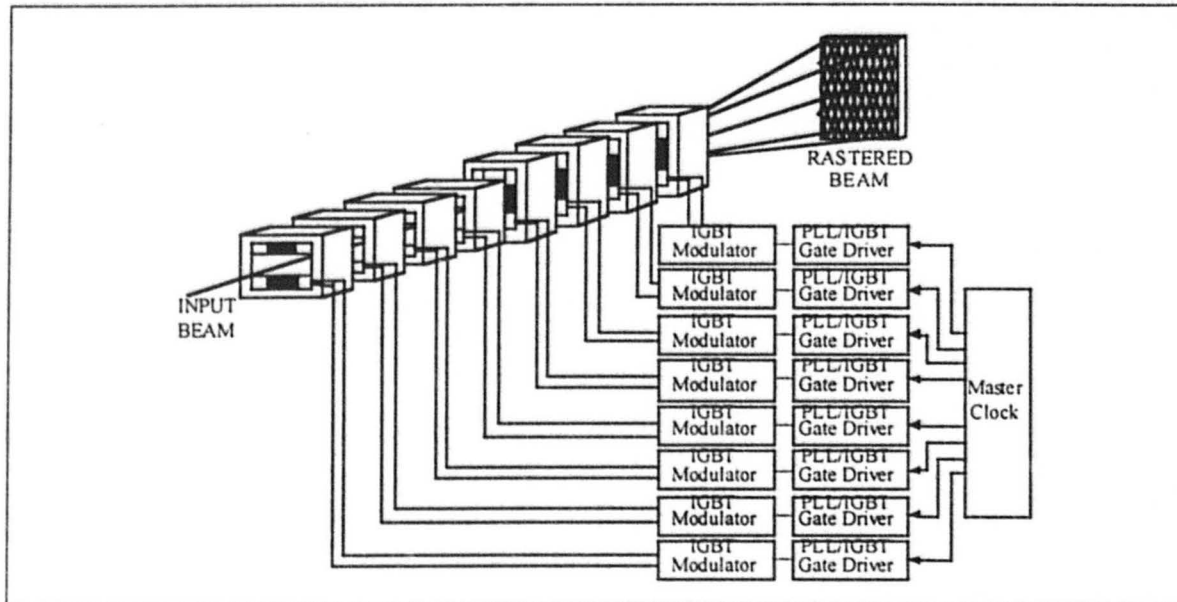
![APT Accelerator Production of Tritium logo]

Figure 3. The arrangement for the eight raster magnets.

To eliminate single-point failure modes that would result in collapse of the raster pattern, each raster magnet operates independently of the others. Each runs on its own uninterruptable power supply (UPS) and on its own crystal oscillator. The four x and four y raster magnets run at different preset frequencies.

To synchronize the phase of the four x and four y raster magnets, the voltage-controlled crystal oscillators in each raster magnet modulator are phase-synchronized to one of two master oscillators, one for x and one for y. Loss of phaselock leads to a graceful degradation of the raster pattern over a period of minutes.

To produce a uniform beam-power density on the tritium-production target, the current waveform for the raster dipole magnets is triangular. Because the raster magnets are very inductive, this triangular waveform is produced by driving them with a voltage square wave. Although a sawtooth current waveform would also work, it would require very high voltages during the flyback phase.

To produce a fine-grain raster mesh at the production target, the x and y raster magnets are run with a frequency ratio of 47 to 53. With the beam spot expanded to 1 cm rms $\times$ 2 cm rms (y) at the production target by the matching quadrupoles, the power density at the target is sufficiently uniform to eliminate spatial thermal stresses.

By running the x and y raster frequencies between 500 and 600 Hz, the thermal transients in the production target are kept under about 6°C.

The 1 cm $\times$ 2 cm rms beam-spot size is small enough to prevent any penumbra outside the 25-cm $\times$ 210-cm region at the target, and large enough to fill-in the 47$\times$53 raster mesh.

5 Raster Magnet Circuit Description

5.1 Block Diagram

Figure 4 shows a block diagram of the circuit for an individual raster magnet. The blocks are named as follows:

- Uninterruptable power supply,
- An ac/dc converter power supply,
- Capacitor bank for energy storage,
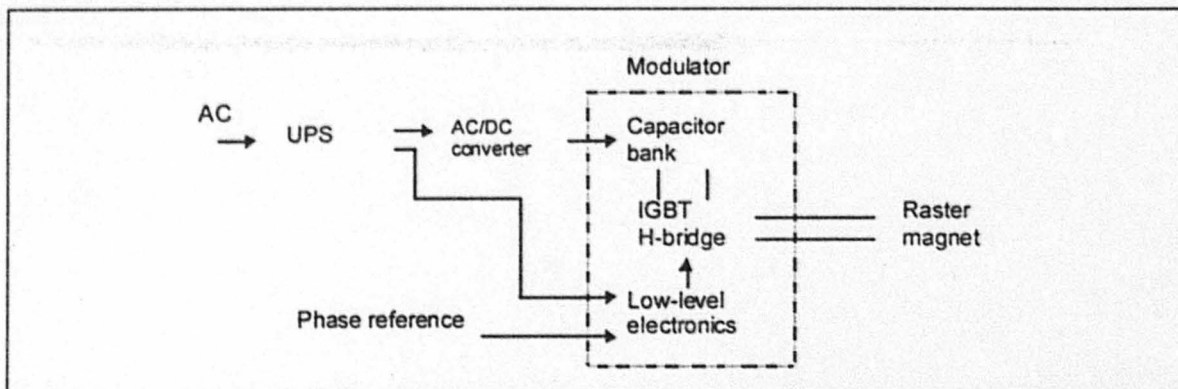- Low-level control circuitry,
- IGBT H-bridge, and
- Raster magnet.

Figure 4. Block diagram of circuit for a raster magnet.

The UPS is a commercially-available unit capable of supplying 1 kW for about 15 minutes. The ac/dc supply is a commercial 300-volt, 6-amp dc voltage-regulated power supply. It maintains a constant charge on the 36-mF (6 × 6 mF), 350-volt-ac-rated capacitor bank. The present design requires about 200 watts of dc power to maintain charge on the capacitors.

5.2 Low-Level Circuitry

The phase-locked loop (PLL) circuit block diagram is shown in Fig. 5. A 1.024-MHz voltage-controlled crystal oscillator is divided down by two 8-bit 74F269 counters, which are preset by four 4-bit hexidecimal switches. The divider output is then divided by a 74113A J-K flip flop to provide a 50% duty cycle raster frequency signal. The output is also fed back to a Motorola 74HC4046A PLL chip, where its phase is compared to the reference

signal. When the phase reference signal is absent, the crystal oscillator runs at its center frequency. These oscillators are all preset to be about ±5 ppm (parts per million).
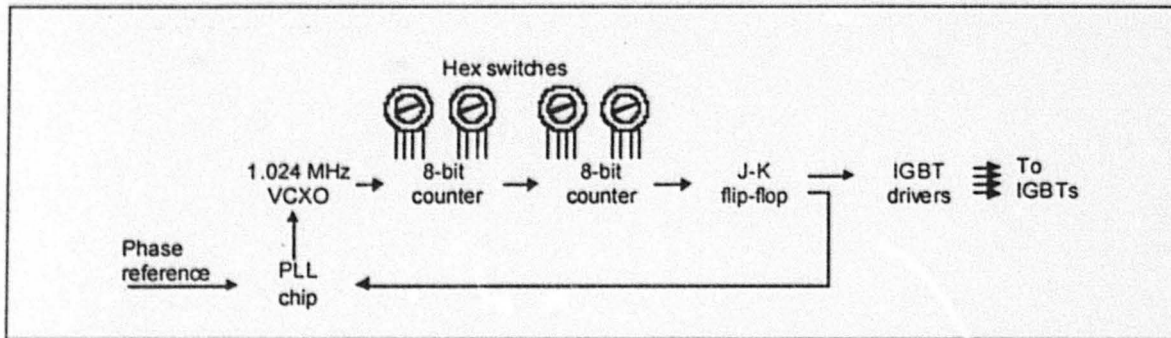

Figure 5. Phase-locked loop block diagram.

5.3   IGBT Circuit

A block diagram of the IGBT H-bridge circuit is shown in Fig. 6. Four Power-X CM200DY-12H IGBTs are driven by the low-level circuitry and produce a 50%-duty-cycle voltage square-wave across the raster magnet. Because the raster magnet is primarily inductive, the current waveform is nearly triangular (the L/R time constant is about 5 ms). The size of the capacitor bank was chosen to limit the voltage fluctuation during the discharge cycle to a fraction of a volt, and also to limit the peak ac current in the individual capacitors. Every half cycle, free-wheeling diodes in the IGBT H-bridge restore the magnetic energy to the capacitors. For this reason, the peak reactive power supplied to the raster magnet is 25 to 30 times higher than the dc power required for keeping the capacitors charged.
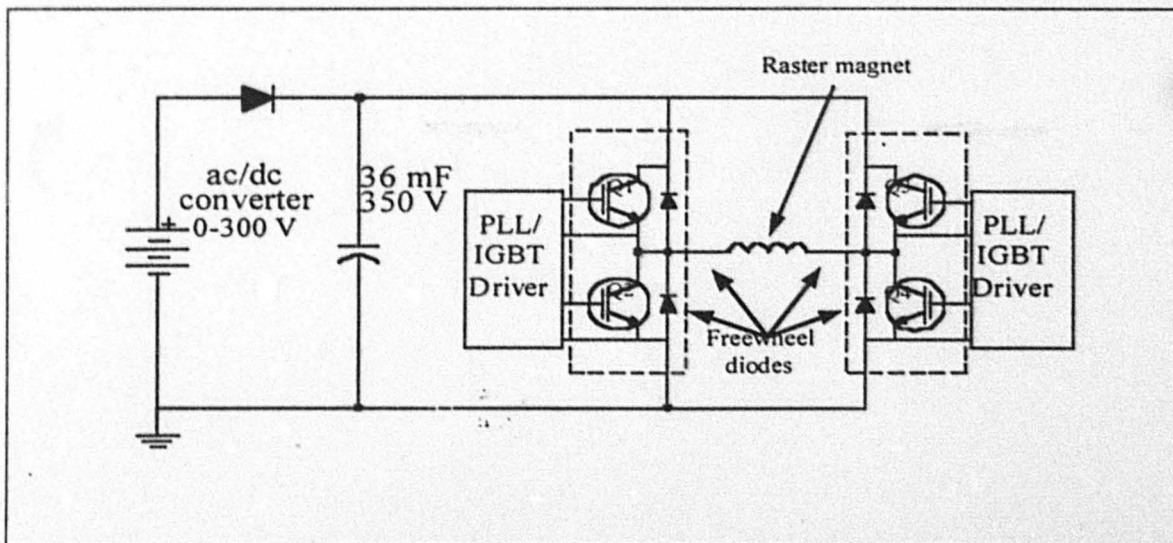

Figure 6. IGBT H-bridge circuit.

5.4 Packaging

Figure 7 shows the rack-mount ac/dc converter chassis and the IGBT modulator chassis. Front panel meters on the voltage-regulated ac/dc converter monitor the dc output current and voltage. The modulator chassis contains the capacitor bank, low-level circuitry, and IGBT H-bridge. Each H-bridge can produce a voltage square wave of up to ±280 volts to the raster magnet. The resulting triangular current waveform is about ±100 amps peak, depending on frequency. Front panel meters on the modulator monitor the raster period and the rms magnet current. LEDs monitor interlocks, dc power, and PLL phaselock status.

Figure 7. The ac/dc supply and modulator chassis.

All the electronics for eight raster magnets are contained in two racks, one for the four x magnets and one for the four y magnets. Oscilliscopes in each rack displays the real-time analog sum of the four B-dot (dB/dt) signals from pickup loops in the raster magnets, as well as the integral of this sum (the triangular B(t) waveform). Because the sum signals are displayed, loss of either the sum amplitude or phaselock is easily seen.

5.5   Raster Magnet

The raster magnet is an H-magnet made of Ceramic Magnetics MN-60 ferrite, 30 cm long, with an 8-cm × 8-cm aperture, as shown in Fig. 8. Two racetrack coils, each with 20 turns, are connected in series. The conductor is 3/16-inch square hollow water-cooled copper conductor. The raster magnet has a dc resistance of about 20 milli-ohms, and an inductance of about 1.2 mH. One hundred amps (4000 amp-turns) corresponds to a peak field of about 620 Gauss. The effective length of the magnet is about 35 cm. Thus, the integrated field is about 0.022 T-m at 100 amps. The IGBT modulator is connected to the raster magnet with 15 meters of 3-gauge stranded copper wire. Each raster magnet contains three 1-turn B-dot (dB/dt) loops wound on one of the poles for monitoring the magnetic field in the gap. The magnet cables each have two Rogowski I-dot (dI/dt) toroids for monitoring the current waveform. These sensors (32 in all) are used for both the visual displays and for the fault-detection circuits.
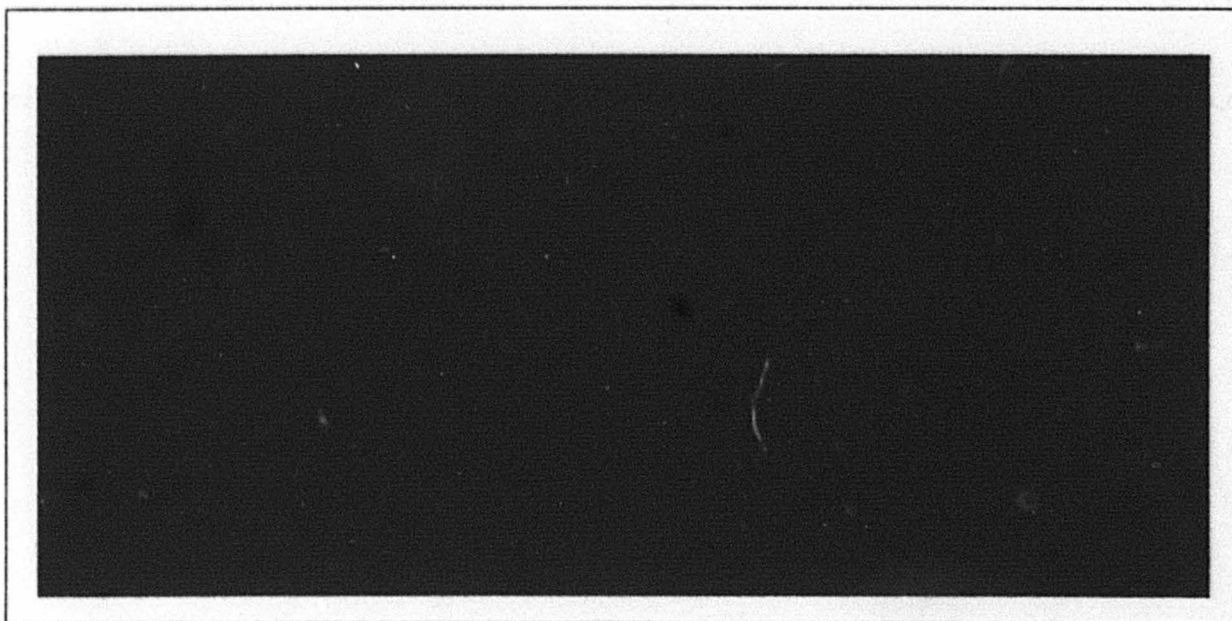

Figure 8. Raster magnets.

5.6   Master Clock

The master clock rackmount chassis contains a voltage-controlled crystal oscillators identical to the units in the IGBT modulator chassis, and two 16-bit binary divide-by-N circuits, one for x and one for y. Like those in the modulators, hex switches are used to preset the output frequencies. Buffered reference output signals are connected to the appropriate IGBT modulators. In addition, the Master Clock contains upper and lower frequency window comparators for monitoring the x and y output frequencies. These comparator signals are ANDed with a 1.024-MHz square-wave signal and distributed to four independent fault-detection circuits.

5.7 Fault-Detection Circuit

Four completely independent fault-detection circuits monitor the 36 input sensors. The sensors are the following:

- 16 B-dot signals (two per raster magnet),
- 16 I-dot signals (two per raster magnet), and
- 4 frequency window comparator signals.

Each fault-detection circuit is independently powered by its own UPS to eliminate single-point failures. For each fault-detection circuit, four x B-dot (or I-dot) signals and four y B-dot (or I-dot) signals are passively added to produce two analog sum signals, one for x and one for y. These sum signals are square waves if all four x or y magnets are in phase. These signals are rectified and filtered with a 10-ms low-pass filter and monitored by window comparators. A phase error of more than 10 ms or an amplitude error of 5% will trip the window comparator. The output of the window comparators are ANDed with one of the four 1.024-MHz frequency window comparator square-wave signals from the Master Clock to produce 1.024-MHz beam-enable signals, which are transmitted by diverse routes to three out of four fault-detection receivers near the linac injector. The receiver logic is shown in Fig. 9.
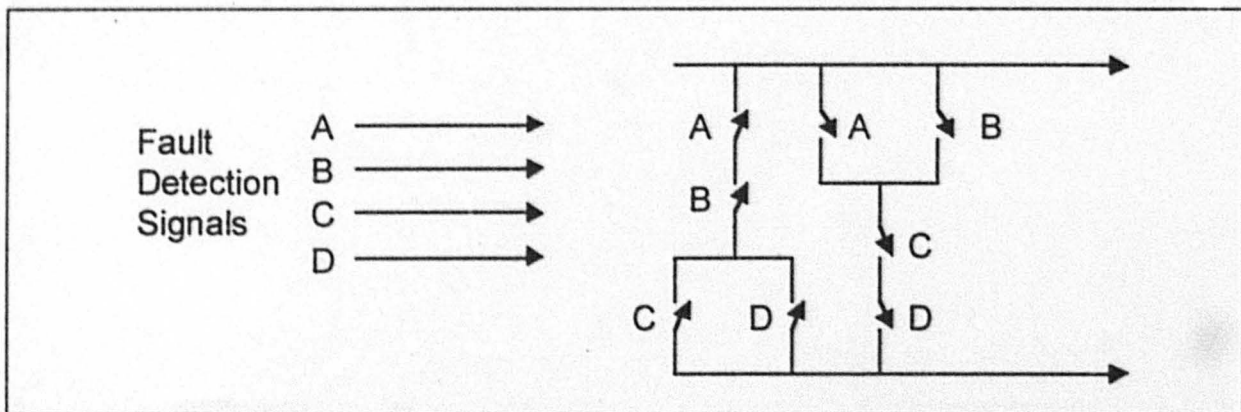

Figure 9. Fault-detection receiver with three out of four logic (relay notation).

These receivers are of the missing-pulse type and can detect loss of the 1.024-MHz square-wave signal in several microseconds. If fewer than three of the four beam-enable signals are valid, then the linac injector will be shut down.

6   Test Results

The primary raster waveforms as measured in an oscilloscope are shown in Fig. 10.
Spikes in the modulator voltage are caused by the unavoidable stray inductances being
switched by the IGBTs in the modulator. Snubber circuits across the IGBTs reduce these
transients to an acceptable level. Because of the freewheeling diodes, the modulator effi-
ciently converts the reactive magnet energy back to voltage to recharge the capacitors.
As an example, 32 kVA (106 A at 300 V) of peak reactive power at 500 Hz requires only
850 watts of real input power. Power loss contributions come from the modulator, the
cabling, and the raster magnet, as follows:

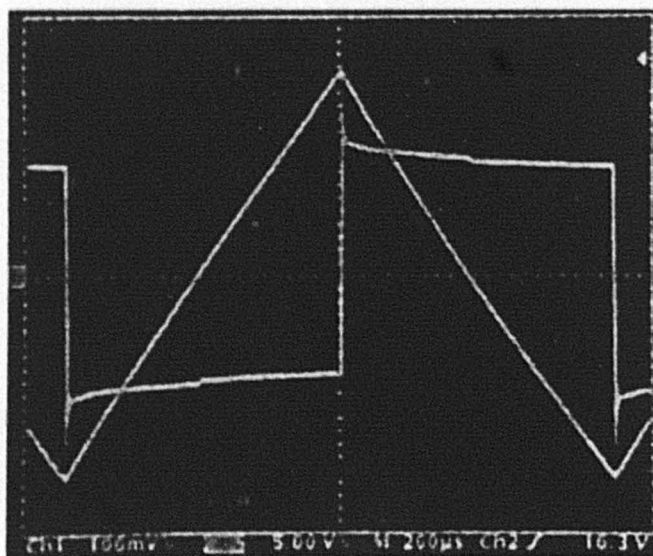|	
Eddy current losses in magnet coil	350 W
Resistive loss in magnet coil	180 W
Voltage drop in IGBTs/diodes	175 W
Resistive loss in 15-m power cable	65 W
Other (hysteresis in ferrite, snubber, etc)	80 W

Figure 10. Measured voltage and current waveforms of modulator.

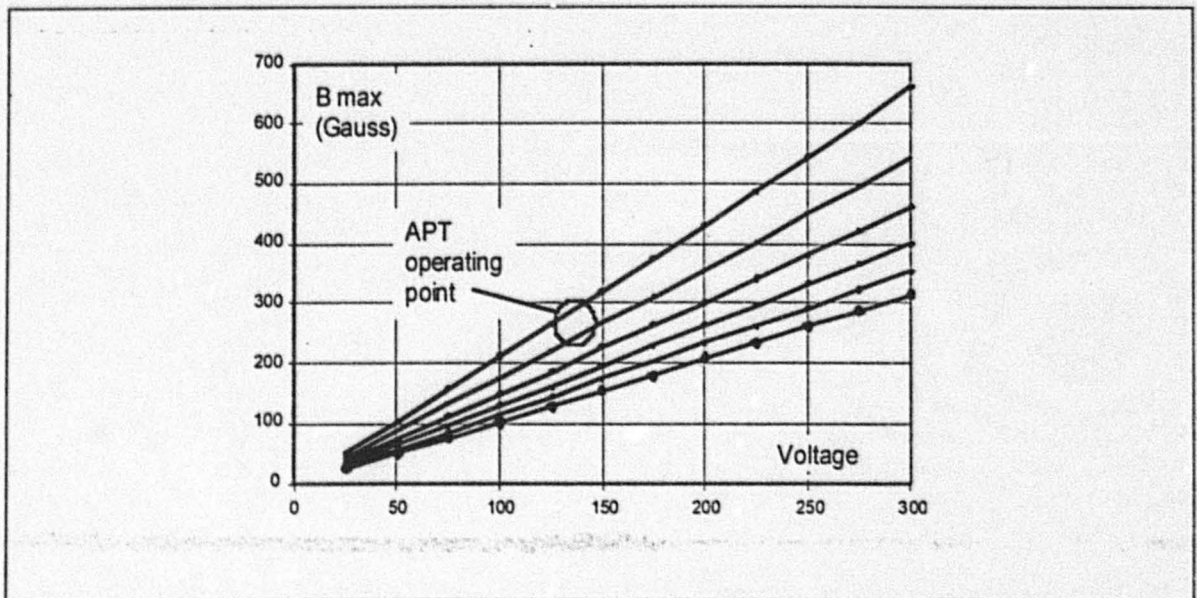Figure 11 shows that the maximum attainable B field is over 600 Gauss at 500 Hz, dropping to 300 Gauss at 1000 Hz.

Figure 11. Maximum B field vs. dc input voltage.

Figure 12 shows a plot of peak reactive power vs. input dc power. Typically, the ratio of peak reactive power to input dc power exceeds 25 to 1.
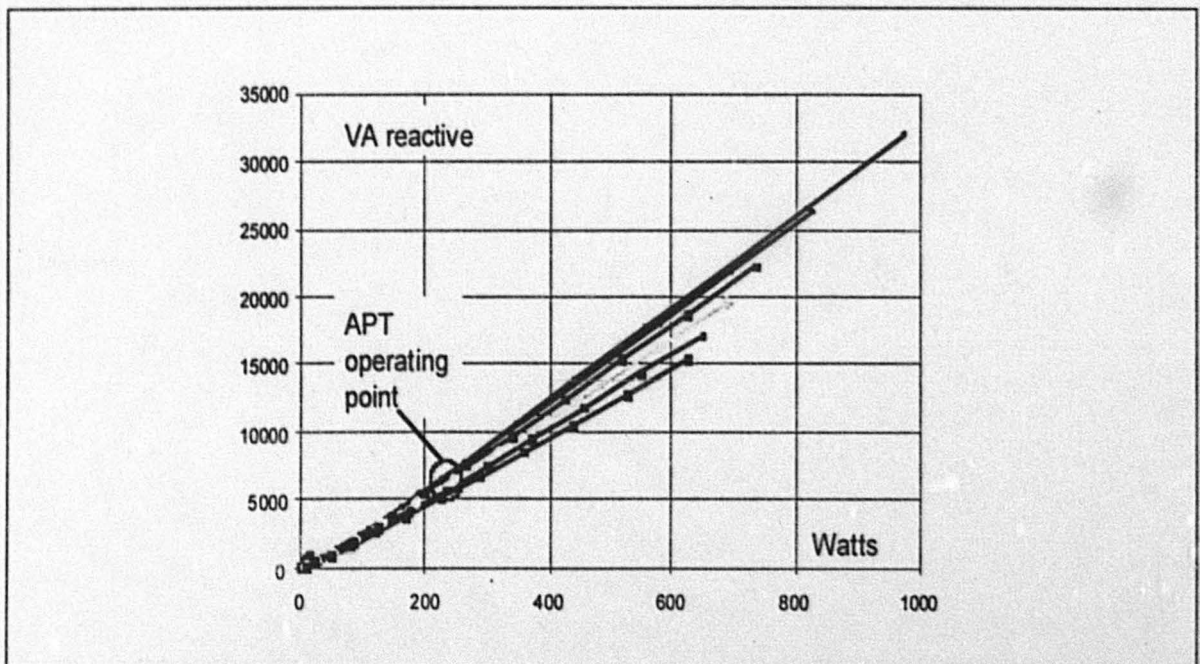

Figure 12. Plot of peak reactive power vs. dc input power.

**Accelerator
Production
of Tritium**

Figures 13 and 14 show the x-y 47×53 raster pattern produced by summing the x and y raster magnet current waveforms. The specific frequencies are 508.441 Hz (x) and 573.348 Hz (y). Figure 13 is a computer simulation, including an L/R droop and a maximum 5-ms risetime expected due to beam tube resistivity. The L/R droop causes a slight curvature of the triangular current waveform. Figure 14 is a photograph of an oscilliscope pattern derived from the pole-tip B-dot coils in all eight raster magnets. The individual B-dot signals were summed and electronically integrated. There is good agreement between the simulated pattern and the actual measured pattern. Simulations (Fig. 15) show that the uniformity of the beam distribution in the 19 cm (h) × 190 cm (v) raster pattern is about ±1% with a 1-cm (h) × 2-cm (v) rms beam spot.
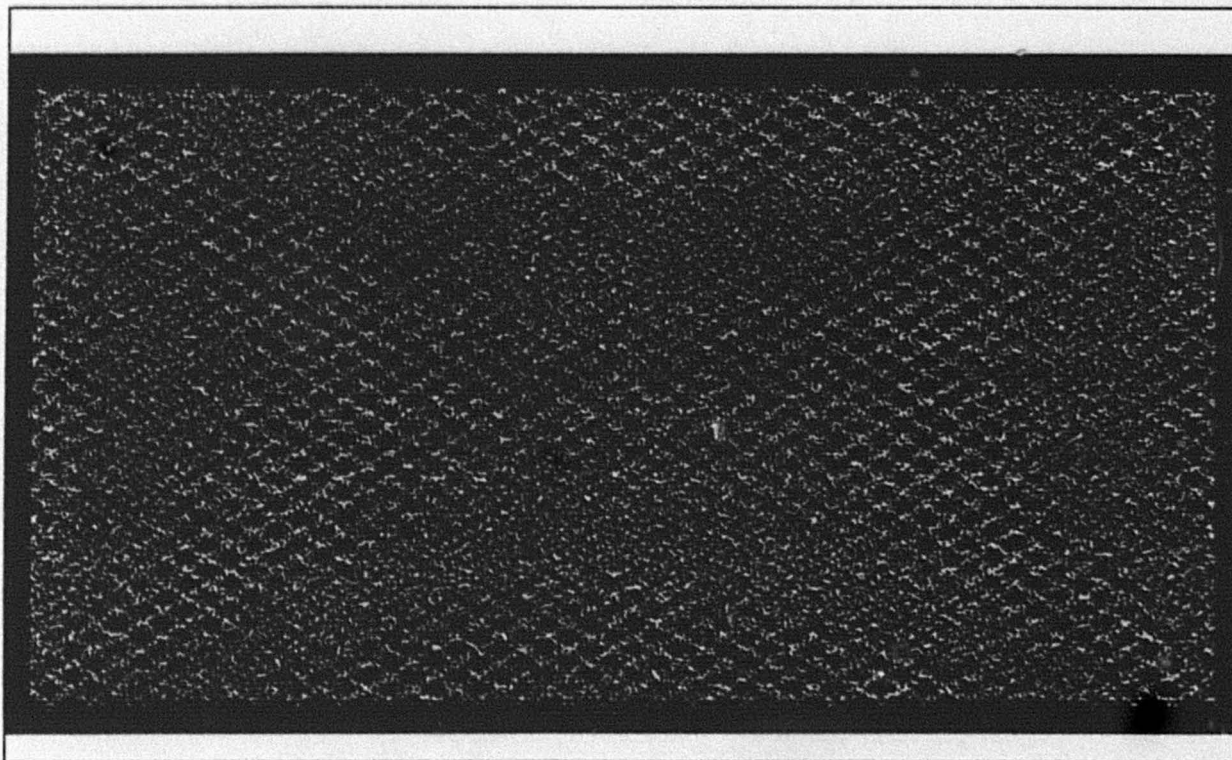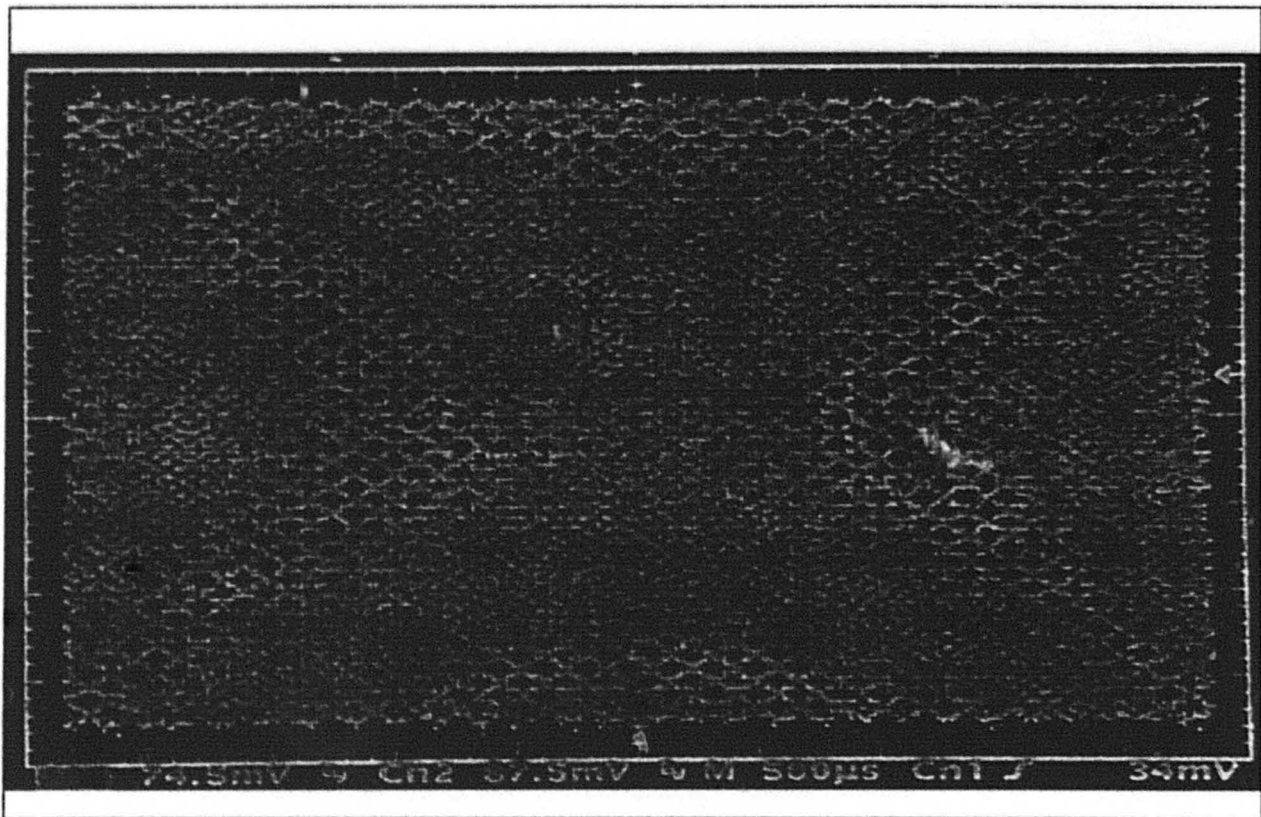

Figure 13. Simulated 47×53 raster pattern.

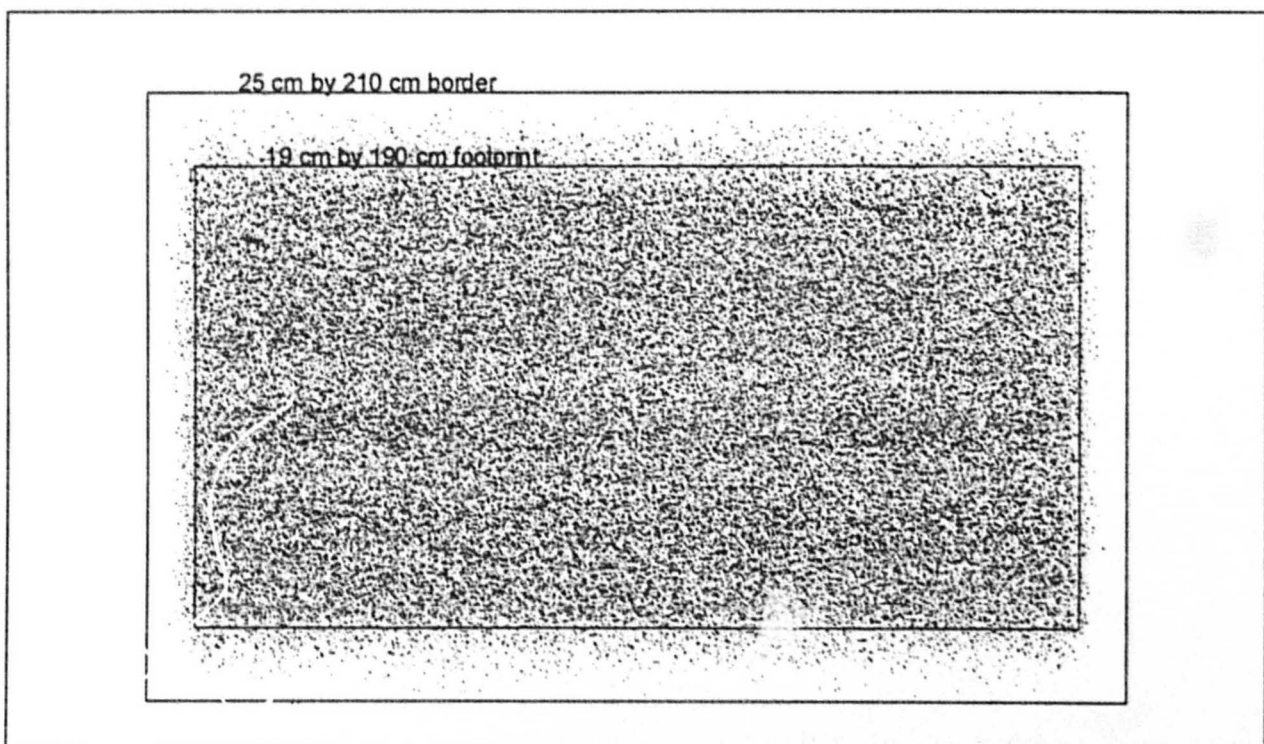Figure 14. Observed 47×53 raster pattern.

25 cm by 210 cm border

19 cm by 190 cm footprint

Figure 15. Expected beam distribution with a 1-cm × 2-cm beam spot.

Accelerator
Production
of Tritium

A ceramic (alumina) beam tube is required inside the raster magnets to eliminate the eddy currents due to rastering. The ceramic tube has a conducting surface, about one skin depth at 350-MHz thick, on the inside to shield the radiofrequency field of the proton beam and to conduct the liberated charge from residual gas ionization.

The effect of a metallic layer on the magnetic field was tested with a 1-mil (25-micron) SS304 nonmagnetic stainless steel tube (2.75-inch diameter), with a resistivity of 77 mohm-cm. The tests were performed with a 620 Gauss peak raster field at 500 Hz. Test results for the power dissipation and the dB/dt risetime inside the tube agreed with the following equations for power loss and risetime:

$$P = \frac{\pi l t a^3}{\rho}\left(\frac{dB}{dt}\right)^2 = 24 \text{ watts, and}$$

$$\tau_{95\%} = 3\tau = \frac{\mu_0 a t}{2\rho} = 2 \ \mu\text{sec} (95\% \text{ risetime}),$$

where l is the raster magnet effective length (35 cm), t is the beam tube thickness (1 mil), a is the beam-tube inside radius (1.375"), $dB/dt = 124$ T/s, and $\rho = 77$ mohm-cm. This test verifies that the rf beam shield will not significantly affect the raster magnet dB/dt risetime inside the ceramic tube, and that the eddy current heating can be convection-cooled (does not need active cooling).

**Accelerator
Production
of Tritium**

7   Possible Failure Modes

The most probable single-point failure modes are complete loss of one of eight raster magnets or loss of phase synchronization. Other possible failure modes include loss of ac power or loss of water cooling to the magnets.

Loss of a single raster magnet can either be gradual (failure of the ac/dc supply) or sudden (failure of the IGBT H-bridge). In the former case, the capacitor bank has enough stored energy to continue rastering for longer than 1 second. In either case, the raster pattern will be reduced to 75% of its normal size in either x or y, resulting in a 33% increase in the overall beam-power density.

Loss of phase synchronization causes the individual modulators to free run at their own preset crystal oscillator frequencies. Because these are preset within about ±5 ppm, the timing drift is on the order of ±5 ms per second. Figure 16 shows the B-dot waveform about 60 seconds after loss of phaselock on all raster magnets. Figure 17 shows a similar picture for the *B(t)* (triangular waveform) signal.
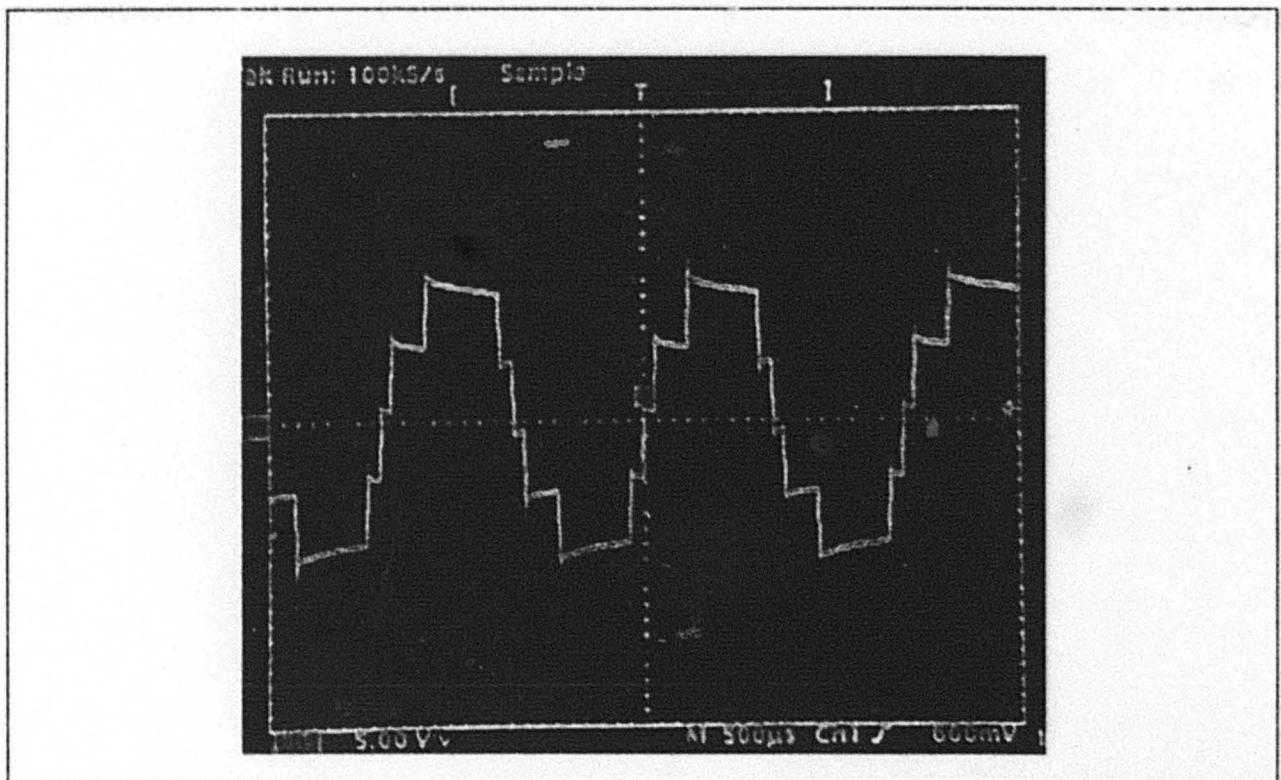

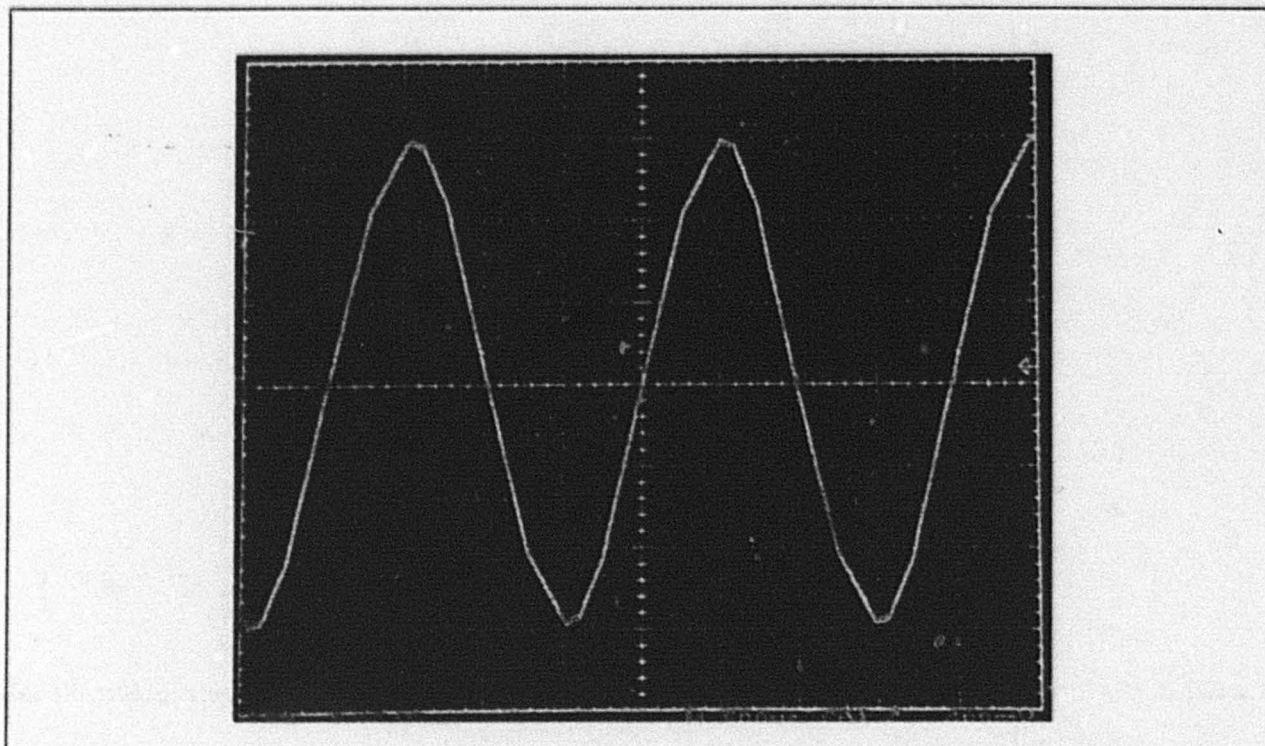**Figure 16. Summed B-dot signal showing loss of PLL synchronization.**

Figure 17. Summed *B(t)* signal showing loss of PLL synchronization.

Loss of ac power is covered by the use of many UPSs: one per raster magnet modulator and dc supply, one per fault-detection circuit, and one for the master clock circuit. Because the magnet thermal interlocks will shut down the associated modulator circuit, this is a potential single-point failure. Using separate water pumps for each magnet will eliminate this single-point failure mode.

All failure modes are detectable by the fault-detection system before any target operating parameter is exceeded.

APT
Accelerator
Production
of Tritium

8 Choice of Operating Parameters

The choice of operating parameters for the beam expander include consideration for:

- Minimization of beam penumbra on target;
- Uniformity of power density on target;
- Limiting the spatial and temporal thermal transients in the target to acceptable values;
- Working well within the safe operating parameter of the raster magnet parameters;
- Minimization of possible beat frequencies with respect to dc magnet power supply ripple; and
- Minimization of possible beat frequencies with respect to any short-duty-cycle pulsed operation of APT.

The final operating parameters were chosen to be:

- Frequency ratio of 47 (h) to 53 (v);
- Horizontal frequency of 508.441 Hz;
- Vertical frequency of 573.348 Hz;
- Peak raster magnet current of 42 A;
- Peak raster magnet field of 260 Gauss; and
- Beam spot size 1-cm rms (h) × 2-cm rms (v).

These operating parameters lead to an estimated maximum thermal transient of about 6°C (±3°), and dynamic mechanical stresses of about 580 psi (4 MPa) peak to peak. In a 100,000,000-particle simulation, the power-density flatness was less than ±2% in any 2.5-mm × 5-mm pixel inside the footprint (except near the border), and less than 0.002% of the particles were observed outside the 25-cm-wide × 210-cm-high window frame. Horizontal and vertical profiles of the simulated expanded beam footprint are shown in Fig. 18 and Fig. 19.
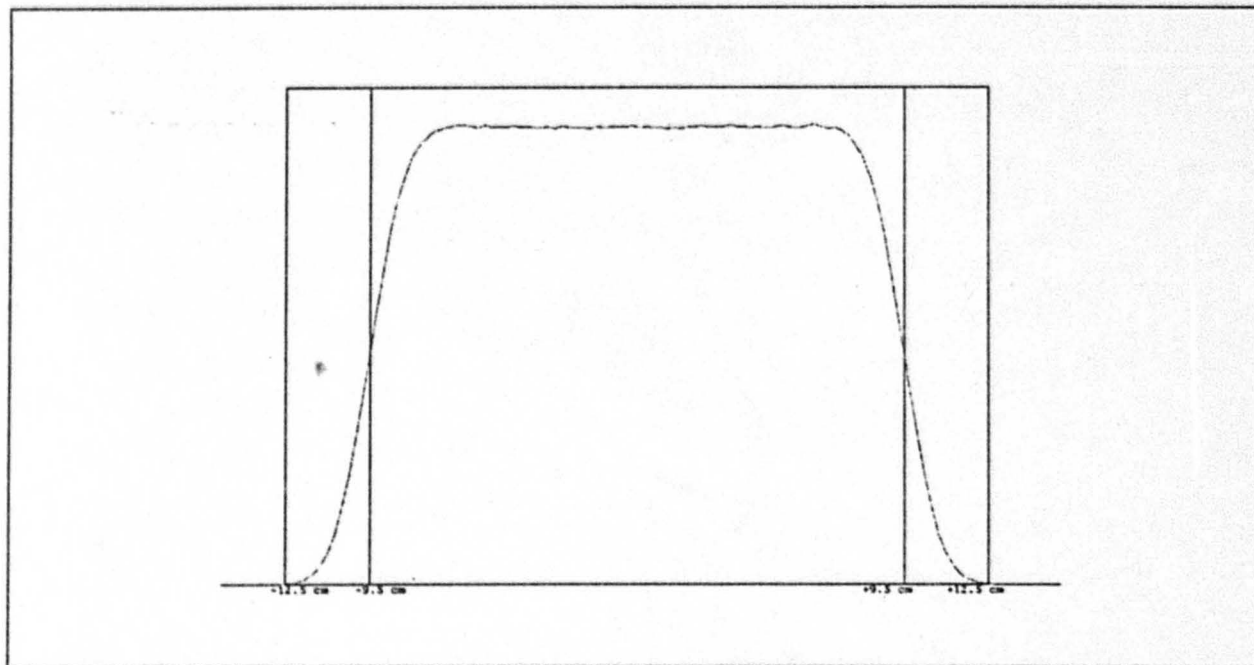
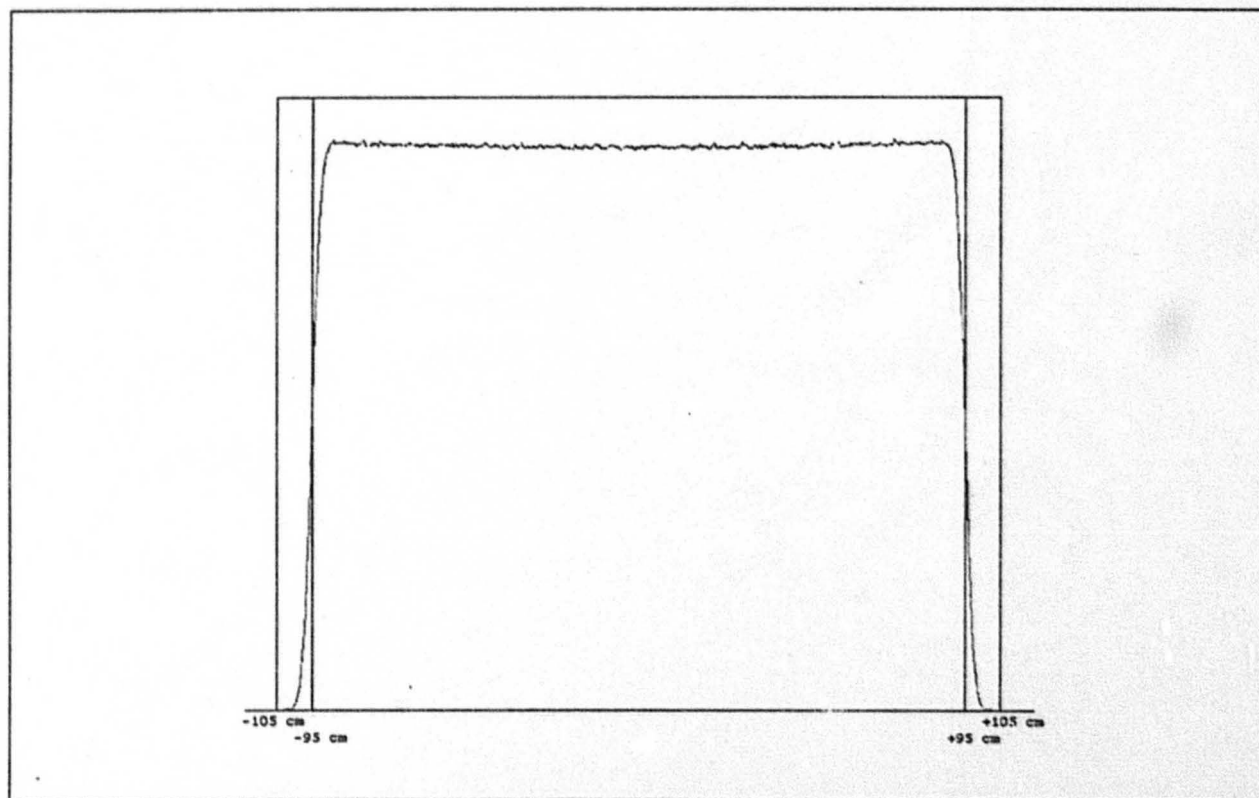**Figure 18. Simulated horizontal profile (top view).**

Figure 19. Simulated vertical profile (side view).

8.1 Beam Diagnostics

The major requirements for the beam diagnostics are the following:

- Continuous operation with full cw beam;
- Determination of expanded beam size to within 5 mm (h) and 3 cm (v);
- Determination of expanded beam centering on target to within similar parameters;
- Determination of rastered beam size in final quad doublet; and
- Determination of specific beam-loss points and times in final quad doublet and in collimator.

Because the beam is rastered in both x and y downstream of the raster magnets, temporal correlation of losses and beam position with the raster frequencies can easily diagnose beam-steering errors. Simple secondary-emission wire harps in front of the neutron spallation target, about 11 wires in each plane, are used in the pulsed mode to determine both the expanded beam size and steering. Measurement of the pulse widths on these wires also determines the rastered beam-spot size at the target. The temporal shape of the beam deflection observed in the beam-position monitors and on the wire harps determines the uniformity of the beam current on the target.

Accelerator
Production
of Tritium

9 Future Work

Both system reliability and power consumption can be improved by replacing the water-cooled hollow copper magnet coil with a stranded Litz wire coil. This will eliminate the water-cooling circuits and substantially reduce the eddy current power loss. Work in this area is progressing.

Long-term testing is required to determine the MTBF of the system. It is believed that the most likely failures will be either in the ac/dc power supplies (MTBF 100,000 hours) or the IGBT (100,000 hours), leading to an estimated 30,000-hour MTBF for each raster magnet, and about 3,500 hours for the complete system.

Accelerator
Production
of Tritium

10 Conclusion

Use of triangular current waveforms, rather than sawtooth waveforms, has eliminated the very high voltages expected if sawtooth waveforms were to be used for rastering. Use of high rastering frequencies permits the use of a square-wave voltage waveform for powering the magnets and limits the thermal transients in the target. Use of eight independently powered raster magnets, synchronized with phase-locked loops, has eliminated the single-point failure concern. Use of freewheeling diodes in the IGBT H-bridge has reduced dc power requirements to a small fraction of the peak reactive power.

11 References

[1] A. J. Jason, B. Blind, and E. M. Svaton, "Uniform Ribbon-Beam Generation for APT," *1988 Linear Accelerator Confterence Proceedings*, p. 192 (1988).

[2] B. Blind, "Generation of a Rectangular Beam distribution for Irradiation of the APT Target," *Proceedings of the 1990 Linear Accelerator Conference*, p. 453 (1990).

[3] U.S. patent number 4,962,317, A. Jason and B. Blind. (1990).

[4] C.R. Rose and R.E. Shafer, "A 200-A, 500-Hz, Triangular Current Wave Modulator and Magnet Used for Particle Beam Rastering," *Proceedings of the 1997 Particle Accelerator Conference*, #7P089 (Vancouver, 5/97).

[5] S. Chapelle, et. al, "Development of a Raster Electronics System for Expanding the APT Proton Beam," *Proceedings of the Linac 98 Conference*, August 98, Chicago, IL.

[6] S. Chapelle, et. al, "Testing a Raster Magnet System for Expanding the APT Proton Beam," *Proceedings of the 1999 Particle Accelerator Conference Conference*, May 1999, New York.